Available online at www.sciencedirect.com
SCIENCE DIRECT®
International Journal of Mass Spectrometry 231 (2004) 1–16
International Journal of Mass Spectrometry
www.elsevier.com/locate/ijms

Escape velocity and resonant ion dynamics in Paul trap mass spectrometers

Glomin Thomas Abraham [a,1], Anindya Chatterjee [b], A.G. Menon [a,*]

[a] *Department of Instrumentation, Indian Institute of Science, Bangalore 560012, India*
[b] *Department of Mechanical Engineering, Indian Institute of Science, Bangalore 560012, India*

Received 13 February 2003; accepted 30 June 2003

Abstract

This paper examines the role of field inhomogeneity in altering trapping strength and ion dynamics within the nominally stable region of Paul trap mass spectrometers. The concept of escape velocity, the minimum velocity required for escape by an ion starting at the center of the trap, has been used to numerically investigate and understand trapping strength variations reported in the literature. The governing equations of motion, in our study, have the form of a pair of weakly coupled and nonlinear Mathieu equations with higher order terms corresponding to hexapole and octopole superpositions. An analytical study of a single (decoupled but representative) nonlinear Mathieu equation has also been carried out to shed light on qualitative aspects of ion dynamics near two important resonances.

The numerical study shows sharp drops in escape velocity near specific β values (β is related to the two Mathieu parameters a and q), with the two largest drops occurring near $\beta = 2/3$ and 1/2. It also shows that the hexapole nonlinearity contributes to the resonance at $\beta = 2/3$, while the octopole nonlinearity does so at $\beta = 1/2$. The analytical study indicates that at the $\beta = 2/3$ resonance the ion is inherently unstable and decreasing nonlinearity has no effect on the net reduction in trapping strength, though it does narrow the region of reduced trapping strength. In the case of the $\beta = 1/2$ resonance, however, the phase portrait indicates only bounded solutions with "escape" occurring when the ion encounters the geometric restriction of the trap. In particular, the reduction in trapping strength near this resonance has been interpreted in terms of the location of a separatrix in the averaged phase space, and its relation to trap size.

Keywords: Paul trap; Ion dynamics; Nonlinear Mathieu equation; Averaging; Escape velocity

1. Introduction

The Paul trap mass spectrometer consists of a three electrode geometry mass analyzer with a central ring electrode and two end cap electrodes [1]. The electrodes are appropriately shaped to produce a linear trapping field within the central cavity when an rf-only or rf/dc potential is applied across the ring and endcap electrodes. The motion of ions, represented by the linear Mathieu equation [2], are uncoupled in the radial and axial directions and ions execute a secular motion whose frequency (in the radial and axial directions) is determined by the Mathieu parameters, a_u and q_u [1], where the subscript u refers to the radial or axial co-ordinate. The mathematical stability of ions is depicted on the Mathieu stability plot which delineates regions on the $a_u - q_u$ plane where both axial and radial motion are stable. The stability region is bounded by values of the parameter β (related through a continuous fraction relation to the parameters a_u and q_u) having values between 0 and 1.

In the pseudopotential well approximation proposed by Dehmelt and coworkers [3,4], along the $a_u = 0$-axis, for small values of q_u, ions can be visualized as oscillating in a parabolic potential well, with trapping strength being determined by the potential at the trap boundary. In practical Paul traps, however, weak higher order fields are known to be superposed on the predominantly linear field on account of both geometric and experimental constraints such as the presence of holes in the endcaps, misalignment in trap ge-

* Corresponding author. Tel.: +91-80-293-2487; fax: +91-360-0683.
E-mail addresses: Glomin_Abraham@ahd.tcs.co.in (G.T. Abraham), anindya@mecheng.iisc.ernet.in (A. Chatterjee), agmenon@isu.iisc.ernet.in (A.G. Menon).
[1] Present address: Tata Consultancy Services, Ashram Road, Ahmedabad, India.

1387-3806/$ – see front matter © 2003 Elsevier B.V. All rights reserved.
doi:10.1016/j.ijms.2003.06.001

ometry, truncation of electrodes to finite size [1,5] stretched [6] and modified hyperbolic angle [7] geometry, as well as space charge caused by trapped ions [8–11]. Although the field inhomogeneities caused by geometric constraints contribute only weak higher order terms to the equation of motion, they have dramatic effects on trap performance [7]. Among the many reported consequences of field inhomogeneities are localized weak spots within the nominally stable trapping region. These are regions where ions do not experience as strong a trapping field as in other regions and here ion motion has a tendency to become unstable. Such observations have resulted in the characterization of regions and points where the trapping strength is low as "black canyons" and "black holes," respectively [12–15]. It has been suggested by Wang et al. [16] that such a phenomenon occurs on account of nonlinear resonance when axial and radial ion secular frequencies and the rf drive frequency have a simple rational relationship with each other. These prior studies have identified the key resonance criteria linking the three frequencies of interest, as well as presented detailed numerical and experimental evidence to show that ion instability does indeed occur at these resonant points. In this paper, we move the analysis further, taking a closer look at the qualitative ion dynamics associated with instability and ejection.

We will first focus on identifying the contribution of specific higher order terms in the trapping field in bringing about lowered trapping strengths in different regions of the Mathieu stability plot. We will then investigate how these specific field inhomogeneties alter ion dynamics and bring about ejection via nonlinear resonances in Paul traps. Both numerical and analytical methods will be used in our study. Two higher order superpositions, the hexapole and the octopole, will be included in the the equations of motion of the trapped ion in the radial and axial directions. Numerical techniques, applied to the governing equations, will profile the trapping strength and highlight the role of hexapole and octopole field inhomogeneities in lowering the trapping strength within the stability plot. The concept of escape velocity, the minimum velocity required by the ion to escape from the trap, will be used to understand experimentally observed trapping strength variations in practical traps. To further understand the dynamics during ion destabilization we will use recent studies [17,18] which deal with the resonant dynamics of a weakly nonlinear parametrically forced equation.

The next section of this paper will develop the governing equations in the radial and axial directions. These equations have the form of coupled nonlinear Mathieu equations with the additional quadratic and cubic terms corresponding to hexapole and octopole field superpositions. Following this, we will present the numerical and analytical techniques used in our study. Finally, we will present the results and discuss the role of field inhomogeneties in altering trapping strength as well as ion dynamics in practical Paul traps.

2. Nonlinear Mathieu equation

The potential distribution within a Paul trap in spherical coordinates assuming axial symmetry, is given by [19,20]

$$\Phi(\rho, \theta, \phi) = (U + V\cos\Omega t)\left[\sum A_N \left(\frac{\rho}{r_0}\right)^N P_N(\cos\theta)\right] \tag{1}$$

where U and V refer to the magnitude of the dc and rf potential, respectively, Ω is the frequency of the rf potential, r_0 is the radius of the ring electrode, P_N are Legendre polynomials, A_N are dimensionless weight factors and ρ denotes the spherical radius coordinate of the ion. In our analysis of the nonlinear field inside the Paul trap, we consider only the hexapole and octopole superpositions along with the ideal quadrupole potential. The Legendre polynomials for the quadrupole, hexapole and octopole potential superpositions (assuming axisymmetric imperfection) are given by Beaty [19]

$$\text{Quadrupole}: \rho^2 P_2(\cos\theta) = \tfrac{1}{2}(2z^2 - r^2) \tag{2}$$

$$\text{Hexapole}: \rho^3 P_3(\cos\theta) = \tfrac{1}{2}(2z^3 - 3zr^2) \tag{3}$$

$$\text{Octopole}: \rho^4 P_4(\cos\theta) = \tfrac{1}{8}(8z^4 - 24z^2r^2 + 3r^4) \tag{4}$$

Substituting these Legendre polynomials into Eq. (1) we get

$$\Phi(r, z, t) = (U + V\cos\Omega t)\left[\frac{A_2}{r_0^2}\left(z^2 - \frac{r^2}{2}\right) + \frac{A_3}{r_0^3}\left(z^3 - \frac{3}{2}zr^2\right) + \frac{A_4}{r_0^4}\left(z^4 - 3z^2r^2 + \frac{3}{8}r^4\right)\right] \tag{5}$$

with A_2, A_3 and A_4, denoting the weight factors of the quadrupole, hexapole and octopole terms in the trapping potential, respectively.

The force $\boldsymbol{F}$ exerted on a particle of charge e by this potential is given by

$$\boldsymbol{F} = -e\nabla_u \Phi \tag{6}$$

and the equation of motion of an ion of mass m is given by

$$m\frac{\mathrm{d}^2u}{\mathrm{d}t^2} = -e\nabla_u \Phi \tag{7}$$

where u represents either the radial (r) or axial (z) coordinate.

Since the inhomogeneties are axisymmetric, by substituting for Φ in Eq. (7) we have the equation of motion of the

ion in the r-direction as

$$m\frac{d^2r}{dt^2} = -e(U+V\cos\Omega t)\frac{\partial}{\partial r}\left[\frac{A_2}{r_0^2}\left(z^2-\frac{r^2}{2}\right) + \frac{A_3}{r_0^3}\left(z^3-\frac{3}{2}zr^2\right)+\frac{A_4}{r_0^4}\left(z^4-3z^2r^2+\frac{3}{8}r^4\right)\right]$$
$$= \frac{eA_2}{r_0^2}(U+V\cos\Omega t) \times\left[r-\frac{3h}{r_0}zr+\frac{f}{r_0^2}\left(\frac{3}{2}r^3-6z^2r\right)\right] \quad (8)$$

where $h = A_3/A_2$ and $f = A_4/A_2$ denote the strength of the hexapole and octopole nonlinearity with respect to the quadrupole term.

Substituting $\tau = \Omega t/2$ into the equation of motion (Eq. (8)) we get

$$\frac{d^2r}{d\tau^2}+(a_r-2q_r\cos 2\tau)\left[r-\frac{3h}{r_0}zr+\frac{f}{r_0^2}\left(\frac{3}{2}r^3-6z^2r\right)\right]=0 \quad (9)$$

where

$$a_r = -\frac{4eA_2U}{m\Omega^2r_0^2} \quad (10)$$

and

$$q_r = \frac{2eA_2V}{m\Omega^2r_0^2} \quad (11)$$

Eqs. (10) and (11) differs algebraically from the expression of a_r and q_r for the ideal case with the appearance of A_2, the weight factor of the quadrupole term in the numerator. In our study, A_2 is set equal to 1 (although a small correction to this value could be incorporated, as pointed out to one us by an anonymous reviewer of another work [21]). The equation of motion in the z direction can be similarly derived as

$$\frac{d^2z}{d\tau^2}+(a_z-2q_z\cos 2\tau) \times\left[z+\frac{h}{r_0}\left(3z^2-\frac{3}{2}r^2\right)+\frac{f}{r_0^2}\left(4z^3-6r^2z\right)\right]=0 \quad (12)$$

where $a_z = -2a_r$ and $q_z = -2q_r$.

Eqs. (9) and (12), which have the form of nonlinear Mathieu equations, governs the motion of ions in practical Paul traps in the radial and axial directions, respectively. The nonlinear and coupling terms arise as a result of the hexapole and octopole superpositions in the expression for the potential function. The form of the nonlinear equation derived above differs from the equation used by Wang et al. [16] principally in the sign associated with some terms on account of our using the potential function given by Beaty [19].

3. Estimation of escape velocities

The concept of escape velocity has been used in dynamics to quantify the strength with which a particle is trapped in a potential well [22]. The escape velocity provides a measure of the kinetic energy needed by the particle of interest, when starting at the center of the well, to escape to "infinity." In the context of Paul traps, we define the escape velocity as the minimum velocity needed by an ion, situated at the center of the trap, to reach the trap's geometric boundary. In a time varying potential such as in Paul traps, for values of q where the pseudopotential well approximation holds, the escape velocity, v_{esc}, may be visualized by the expression

$$\tfrac{1}{2}mv_{esc}^2 = eD \quad (13)$$

where D, the Dehemelt potential [2] is given by

$$D = \frac{eV^2}{4m\Omega^2z_0^2} \quad (14)$$

At higher values of q, however, where the pseudopotential well approximation fails, it may still be possible to define an effective or equivalent potential, as has been shown by Sudakov [20]. However, here we have avoided such intermediate steps and directly considered the minimum kinetic energy needed by an ion at the center of the trap to reach the trap boundary. This minimum depends on when the ion starts its escape in relation to the phase of the rf potential; the associated calculation is described below. Since all computations have been performed for a fixed mass, m, the results are reported in terms of velocity rather than kinetic energy.

As the equations of motion are of second order, to integrate them numerically we need four initial conditions at some time $t = t_0$. These initial conditions are position (r, z) and velocity $(\dot{r}, \dot{z})$ in the r and z-directions. Since the ion is located at the center of the trap, the initial coordinates (r, z) are chosen to be $(0, 0)$. The initial $\dot{r}, \dot{z}$ are computed from a choice of the initial velocity magnitude and its angular direction in the r–z plane. Eqs. (9) and (12) are numerically integrated for a given initial velocity magnitude, at a given initial angle in the r–z plane, and a given choice of t_0 (or, phase of the forcing term). Then the initial velocity magnitude is iteratively adjusted so that the ion *just* reaches the trap boundary within a prespecified "large" time. In our study, the time chosen was large enough so that further increase in the time did not change the result appreciably. This issue will be discussed further, later in the paper. This minimum velocity was repeatedly determined for the angle in the r–z plane varying from 0 to 2π in 12 steps and, for each of these cases, for the phase of the cosine term varying from 0 to 2π in 16 steps. Of these 192 values the minimum is taken as the escape velocity at the chosen (a_z, q_z) pair in the Mathieu stability plot. In our simulations we used the fourth order Runge–Kutta method available in MATLAB (Version

5.3) [23]. We fixed the minimum relative tolerance as 10^{-4} since further decrease in the tolerance limit did not alter the results appreciably.

4. Analytical study

Eqs. (9) and (12) cannot be solved in closed form. Some characteristics of the motion of ions in nonlinear fields have, however, been reported in experimental [15,24,25] and theoretical [7] studies and our analytical study will rely on these features to understand ion dynamics. It was seen that nonlinear resonance occurred when there was a simple rational relationship between the axial, radial and rf drive frequency. For instance, the two major regions of instability [12,13] were seen to have β values of $1/2$ and $2/3$ implying that the secular frequency was 1/4 and 1/3 of the rf drive frequency, respectively.

In a recent study [18] that focuses on analytical treatment of Eq. (12) with $r = 0$, it was seen that in narrow regions in parameter space where solutions are nearly periodic, it is possible to obtain approximate analytical expressions to describe the dynamics. The equation of motion is seen as a linear equation with a small nonlinear perturbation. It is assumed that the linear unperturbed equation has two independent periodic solutions of period T. Any general solution of the linear equation can then be written as a weighted sum of these two independent solutions, the weights being constants dependent on initial conditions. In the method of approximate averaging used [18] one assumes that the perturbed equation also has a similar solution, but with the previously constant weights now becoming time dependent. The averaging technique helps one determine how the weights vary with time and thereby characterizes the solutions. For completeness, the key points of the technique are given below.

Let us consider the nonlinear Mathieu equation (for axial motion) written in the form

$$\frac{\mathrm{d}^2 z}{\mathrm{d}\tau^2} + (a_z - 2q_z \cos 2\tau)z = \varepsilon F(z, \dot{z}, \tau) \tag{15}$$

where F is π-periodic in the τ variable and represents a perturbation to the linear Mathieu equation; the smallness of the perturbation is signified by $0 < \varepsilon \ll 1$.

The solutions of the unperturbed equation (putting $\varepsilon = 0$ in Eq. (15)) are special functions known as Mathieu functions [26,27] which are represented as

$$z = A \sum_{n=-\infty}^{\infty} C_n \cos(\beta + 2n)\tau + B \sum_{n=-\infty}^{\infty} S_n \sin(\beta + 2n)\tau \tag{16}$$

where A and B are arbitrary constants, C_n and S_n are recursively defined constant coefficients in the Mathieu functions, and β is related to the Mathieu parameters a_u and q_u [1]. The solution to the perturbed equation (that is, when $\varepsilon \neq 0$) can be assumed to have a similar form but now A and B are assumed to vary slowly with time and the solution is expressed as

$$z = A(\tau) \sum_{n=-\infty}^{\infty} C_n \cos(\beta + 2n)\tau + B(\tau) \sum_{n=-\infty}^{\infty} S_n \sin(\beta + 2n)\tau \tag{17}$$

For those special (a_u, q_u) points such that β is rational, Eq. (16) is periodic (with some period T). For sufficiently small ε (in Eq. (15)) the averaged solutions of $A(\tau)$ and $B(\tau)$ are given as [18]

$$\dot{A} = \frac{1}{T} \int_0^T \frac{\varepsilon f g_2}{\dot{g}_1 g_2 - \dot{g}_2 g_1} \mathrm{d}\tau \tag{18}$$

and

$$\dot{B} = \frac{1}{T} \int_0^T \frac{\varepsilon f g_1}{\dot{g}_2 g_1 - \dot{g}_1 g_2} \mathrm{d}\tau \tag{19}$$

Truncating the Fourier series in Eq. (17), we write

$$g_1 \approx \sum_{n=-3}^{3} C_n \cos(\beta + 2n)\tau \tag{20}$$

and

$$g_2 \approx \sum_{n=-3}^{3} S_n \sin(\beta + 2n)\tau \tag{21}$$

where C_n and S_n are determined by a Galerkin procedure [18]. The integral on the right hand side of Eqs. (18) and (19) needs to be evaluated to obtain the "slow flow." As in [18], the integration was performed using a harmonic balance approximation and the associated algebra was carried out with the help of a commercial software package MAPLE [28].

5. Results and discussion

The simulations carried out in the present paper have considered a Paul trap with a radius of the ring electrode (r_0) as 7 mm and distance between the endcap electrodes ($2z_0$) as 10 mm. The frequency of the rf drive, Ω, has been fixed at 1 MHz and the mass-to-charge of the trapped ion was taken to be 78 Th. In all simulations except one, the dc potential U was set to zero. The rf voltage V_0–p was varied to obtain different q_z values used in the simulations.

5.1. Numerical simulation

Figs. 1–6 are plots of escape velocity versus q_z. Except for Fig. 3, all plots are along the $a_z = 0$-axis. Figs. 1–3 provide absolute values of escape velocities obtained in our simulations whereas Figs. 4–6 plots the *difference* in escape velocity between the ideal trap and the practical trap. These latter plots have been derived from plots similar to Figs. 1–3.

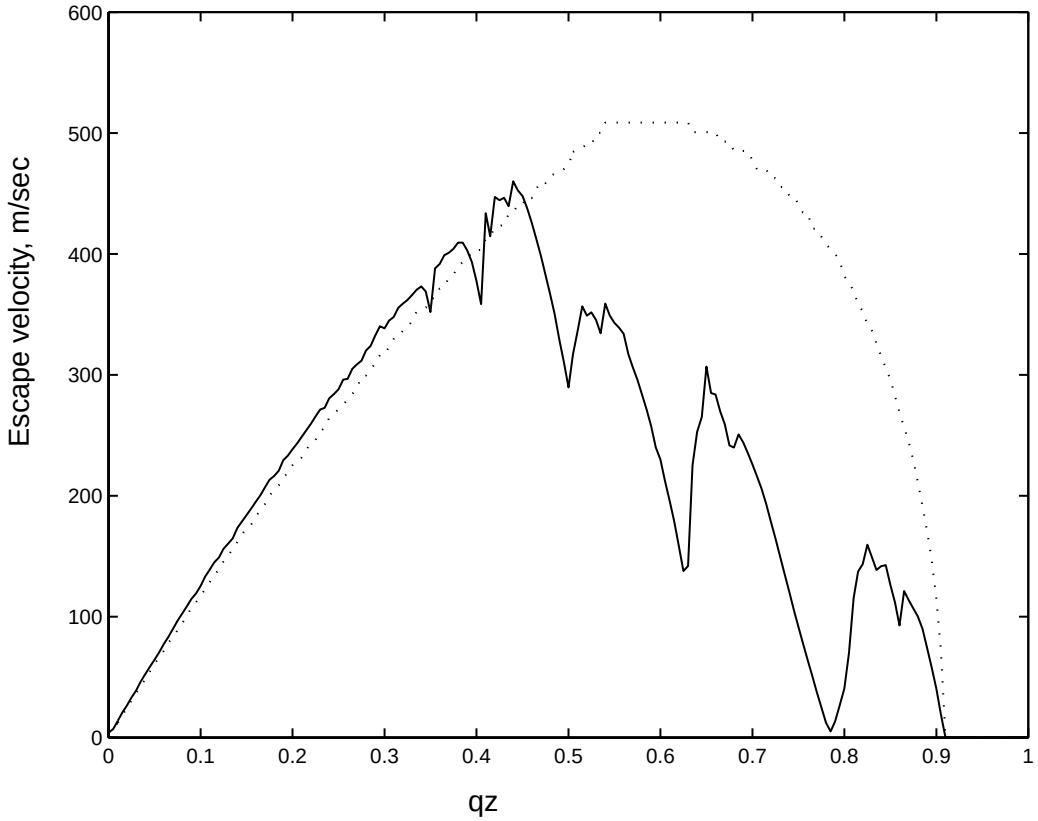

Fig. 1. Escape velocity vs. q_z for 10% hexapole + 10% octopole nonlinearity (solid line). Dotted line refers to ideal case.

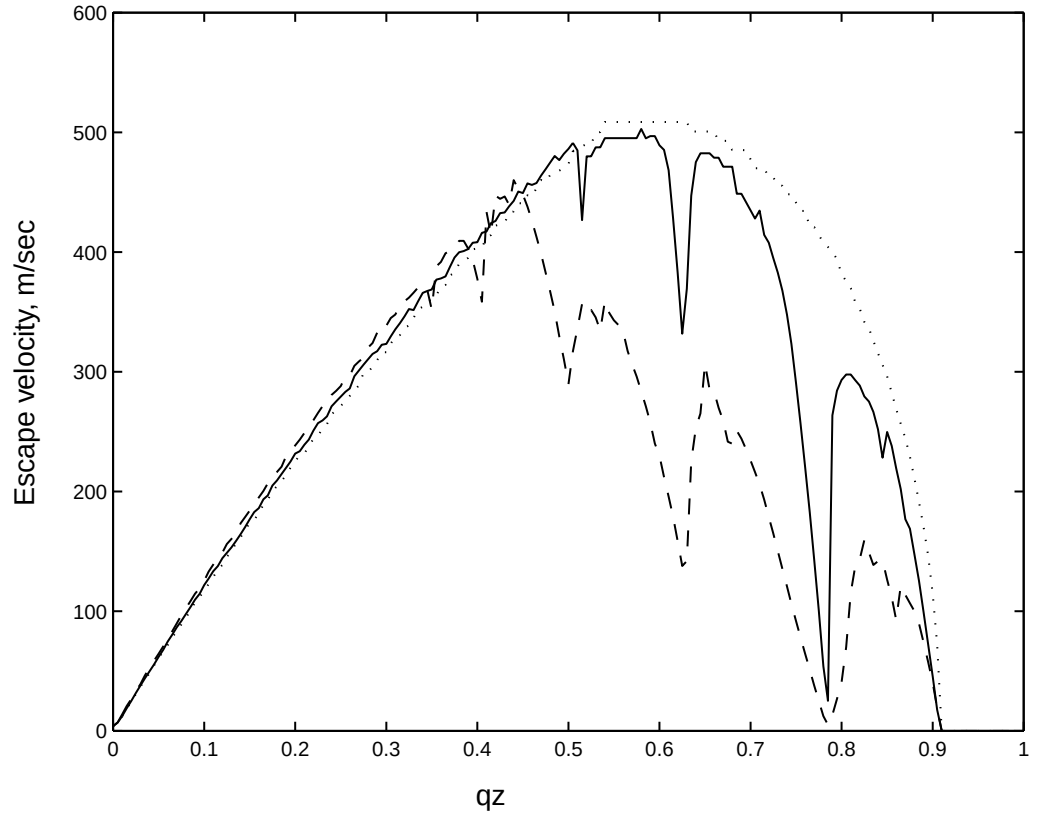

Fig. 2. Escape velocity vs. q_z for 2% each (solid line) and 10% each (dashed line) hexapole + octopole nonlinearity (solid line). Dotted line refers to ideal case.

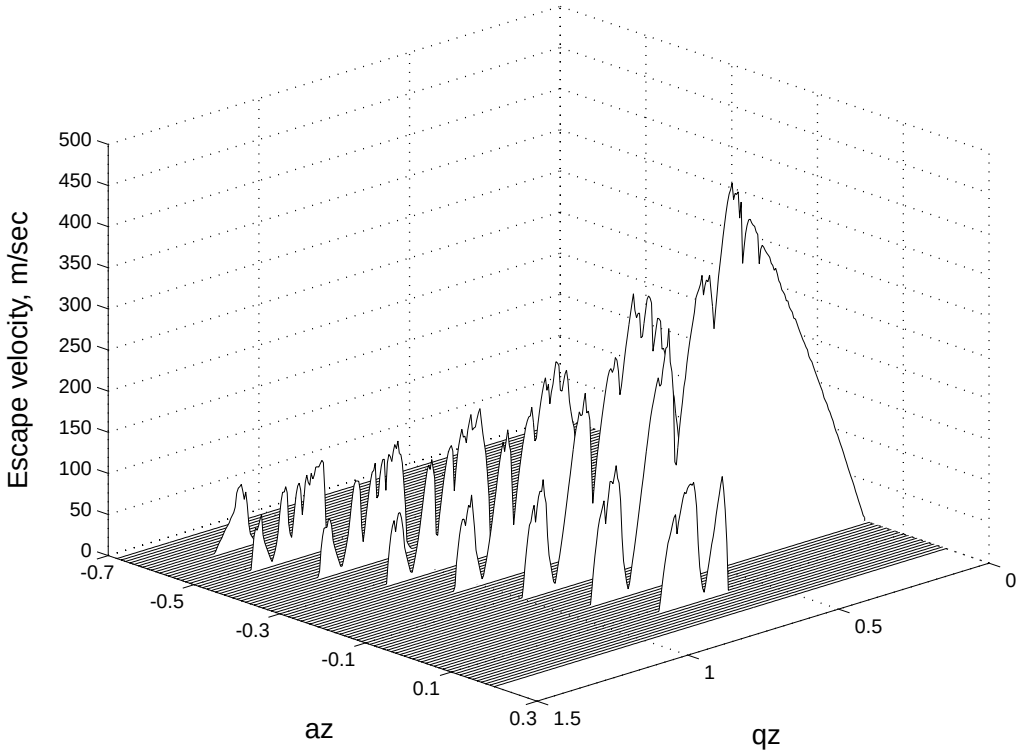

Fig. 3. Escape velocity on the a_z–q_z plane for +10% hexapole and +10% octopole nonlinearity.

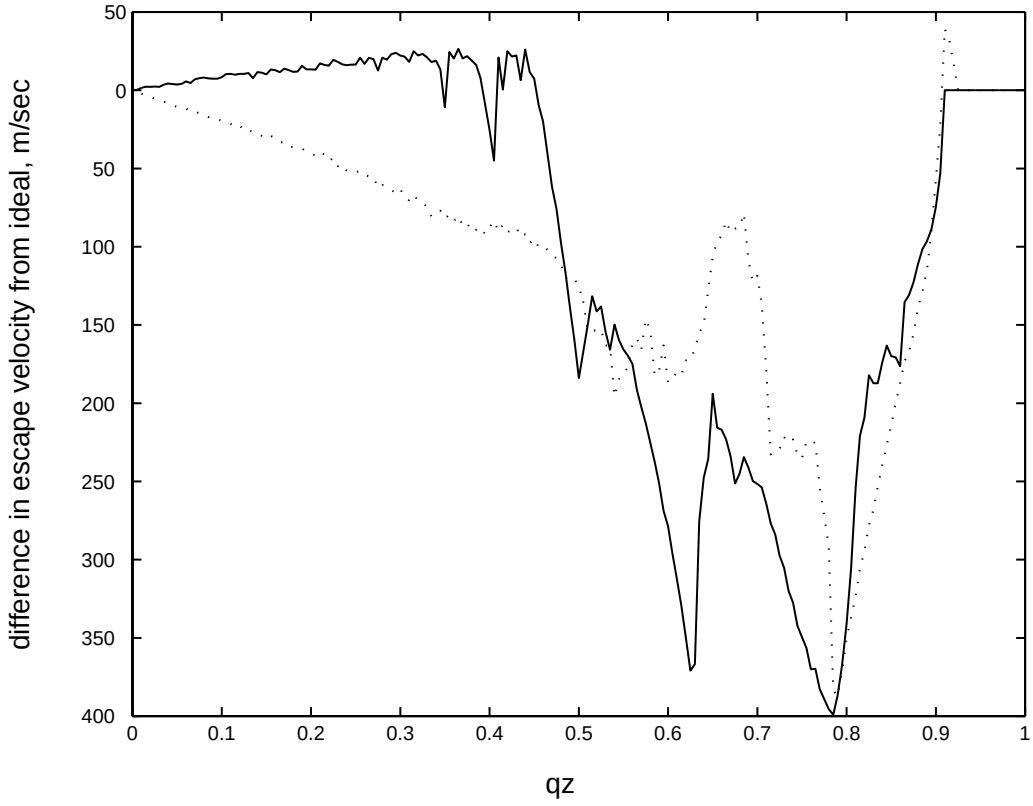

Fig. 4. Difference in escape velocity from ideal trap for +10% hexapole and +10% octopole nonlinearity (solid line). Dotted line refers to −10% hexapole and −10% octopole nonlinearity.

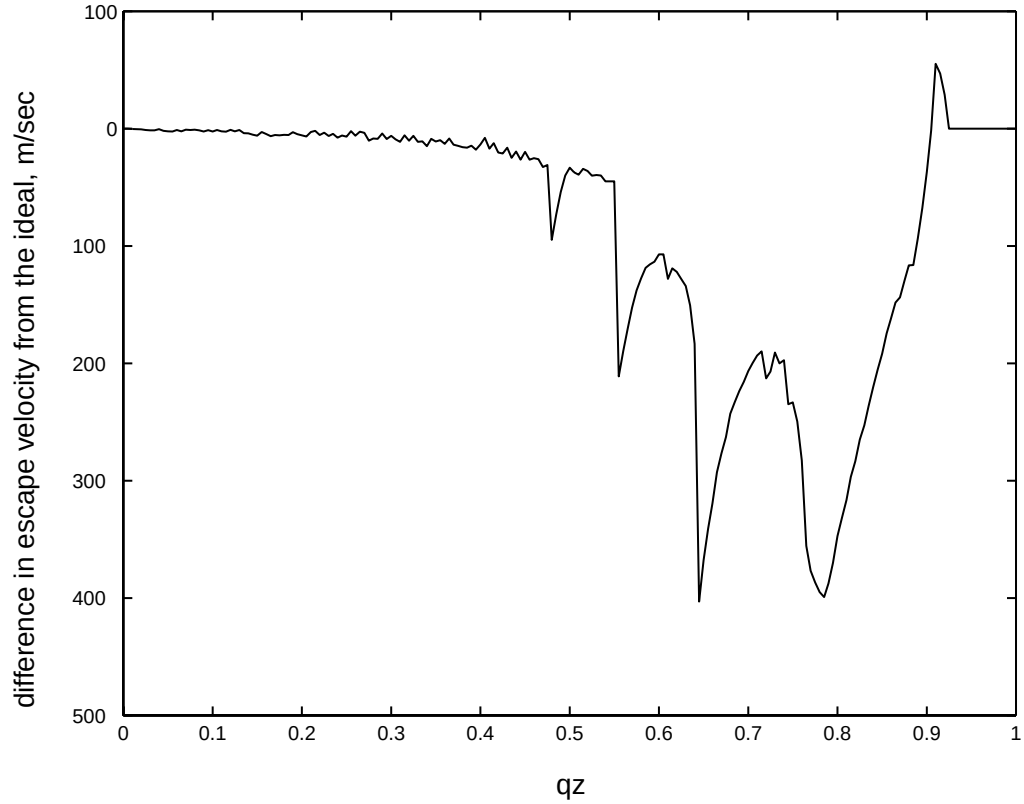

Fig. 5. Difference in escape velocity from ideal trap for +10% hexapole nonlinearity (solid line). Dotted line refers to −10% hexapole nonlinearity. The two lines appear indistinguishable in the plot.

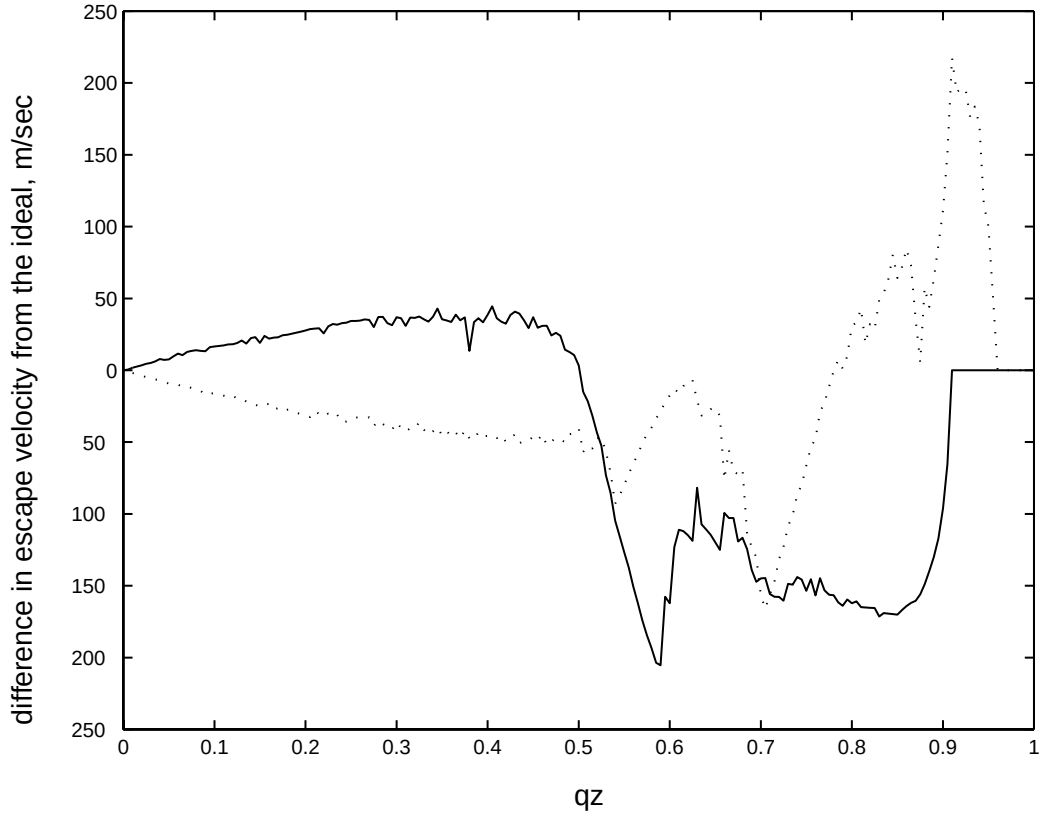

Fig. 6. Difference in escape velocity from ideal trap for +10% octopole nonlinearity (solid line). Dotted line refers to −10% octopole nonlinearity.

For instance, the solid line in Fig. 4 has been derived from the escape velocity values for the practical and ideal case plotted in Fig. 1. Consequently, although we have not provided plots showing the effect of hexapole and octopole inhomogeneity explicitly, they can be visualized from the difference plots presented in Figs. 5 and 6. A value of 10% inhomogeneity has been chosen in these computations to exaggerate the effects that were observed (realistic values of weight factors in practical Paul traps are given in [7]).

Fig. 1 presents the escape velocity versus q_z curve along the $a_z = 0$ line for +10% hexapole and +10% octopole superposition. The dotted line corresponds to the escape velocity for the linear Mathieu equation. We see that the nonlinearity makes the magnitude of escape velocity uneven along q_z with strong minima at q_z values close to 0.5, 0.63 and 0.78. The lowest escape velocity is associated with q_z value close to 0.78 where the escape velocity appears to approach zero. The experimental observations of "black holes" in the Mathieu stability plot were first made at $q_z = 0.78$ and $q_z = 0.63$ along the $a_z = 0$-axis [12,13]. On comparing the observed trapping strength with the ideal equation we see that for low values of q_z ($q_z \lesssim 0.45$) the trapping strength is higher for the nonlinear equation compared to the linear equation except for two points close to $q_z = 0.35$ and $q_z = 0.405$. However, for higher values of q_z the trapping strength is lower for the nonlinear equation as compared to the linear equation with sharp minima at the specific q_z indicated above.

The overall influence of the weight of nonlinearity on escape velocity decreased with decreasing weight of nonlinearity except at $q_z = 0.78$. Fig. 2 presents escape velocity versus q_z curves for +2% hexapole and +2% octopole superposition (solid line). For comparison, the curve corresponding to +10% hexapole and +10% octopole superposition (dashed line) has also been included. It can be seen that decrease in nonlinearity increases the trapping strength throughout the q_z-axis except at the q_z value close to 0.78, where the escape velocity was a minimum, remained unaltered. An additional point to be noted is that although the escape velocity is unaltered at this point, the curve has become sharper.

Fig. 3 plots escape velocity versus q_z for different values of a_z on a three-dimensional plot. In these computations nonlinearities were fixed as +10% hexapole and +10% octopole superposition for a_z values ranging from +0.1 to −0.6 in steps of 0.1. It may be seen that nonzero a_z values retained the undulations in trapping strength which was seen at $a_z = 0$ above, although the magnitude of escape velocity reduced on either side of the $a_z = 0$-axis. Fig. 3 compares favorably with the experimental plot of Guidugli et al. [14].

Fig. 4 plots the difference in trapping strength between an ideal trap and a trap having both hexapole and octopole nonlinearities, the solid line corresponding to +10% hexapole and +10% octopole nonlinearity and the dotted line corresponding to −10% hexapole and −10% octopole nonlinearity. It can be seen that while both the curves shows a sharp minimum at q_z value close to 0.78, at q_z value close to 0.64 the escape velocity curve with positive nonlinearity shows a sharp minimum while that for negative nonlinearity shows a broader minimum.

Fig. 5 is a plot of the difference in trapping strength between an ideal trap and a trap with +10% hexapole superposition. The escape velocity is insensitive to the sign of the hexapole nonlinearity and consequently the behavior of the negative hexapole nonlinearity is identical to the one shown in Fig. 5. The escape velocity in the presence of hexapole superposition is below the escape velocity for the ideal trap for all values of q_z till q_z close to 0.9 and ion destabilization takes place at a q_z value close to 0.925. There are sharp minima at q_z values close to 0.5, 0.64 and 0.78. Although the magnitude of the escape velocity at q_z value close to 0.78 is much lower than that at 0.64 (please refer Fig. 1) the escape velocity *difference* with respect to the ideal trap at both these q_z values is almost the same with the one close to 0.64 being sharper than the one at 0.78.

Fig. 6 plots the difference in trapping strength between an ideal trap and a trap having +10% octopole superposition. The dotted line corresponds to negative octopole nonlinearity and the solid line corresponds to the curve for positive octopole nonlinearity. For lower values of q_z the curve for the positive octopole superposition shows a positive slope while that for the negative nonlinearity shows a negative slope indicating that positive octopole superposition has a stabilizing effect on ion motion at low q_z values. At q_z values greater than 0.5 the escape velocity for the positive octopole nonlinearity becomes lower than the escape velocity for negative nonlinearity and has a minimum at q_z value close to 0.6. The difference (for positive octopole nonlinearities) is confined to a narrow range of q_z values ranging from 0.7 to 0.9 and goes to zero at a q_z value close 0.91. For negative octopole superposition the escape velocity is lower than the ideal case and shows sharp minima at q_z values close to 0.55, 0.7 and 0.87. The escape velocity curve shows a stabilizing effect at q_z values greater than 0.8 for negative octopole superposition, going to zero only at a q_z value close to 0.96 at which point the ion gets destabilized from the trap.

For nonlinear Paul traps, our simulations have reproduced the experimentally observed undulations [12–15] within the stability plot, and also reproduced the shift in the effective boundary of the stability region in the nonlinear Paul trap [20,21]. We also note that, even in *ideal* Paul traps, the trapping strength is not constant but instead smoothly varies throughout the stable region, going to zero at the nominal stability boundaries of $\beta_u = 0$ and 1, and with a maximum somewhere in the middle (e.g., along the $a_z = 0$-axis the maximum occurs close to $q_z = 0.6$).

In the context of weakly nonlinear Paul traps, our simulations have additionally provided insights into the role of both magnitude and sign of hexapole and octopole nonlinearities in ion ejection dynamics near nonlinear resonance points within the stability plot. Several regions of reduced trapping

strength have been seen in the simulations. Of these, two prominent nonlinear resonances occur at q_z values close to 0.64 and 0.78. Although in absolute terms these resonances have widely different escape velocities, the difference of the escape velocity from the ideal (purely linear) case is comparable for the two resonances. Note, however, that they respond to changes in magnitude of nonlinearity in qualitatively dissimilar ways. The $q_z = 0.64$ resonance, for instance, becomes weaker with decrease in magnitude of nonlinearity while the $q_z = 0.78$ resonance becomes sharper, though not weaker at the resonance point.

We will next present results of an analytical study carried out to understand the ion dynamics associated with nonlinear resonances at these two q_z values. The analysis will be motivated and guided by numerically generated Poincaré maps, as described below.

5.2. Analytical study

Poincaré maps were obtained by strobing the phase portrait at periodic intervals corresponding to the time period of the rf drive at two specific points, $(a_z, q_z) = (0, 0.78)$ and $(a_z, q_z) = (0, 0.64)$. In Fig. 7 we present the Poincare map at the $(a_z, q_z) = (0, 0.78)$ using the initial condition $(z, r, \dot{z}, \dot{r}) = (0.00038, 0.00038, 0, 0)$. We can see that the motion is unstable in the z direction and the amplitude of the solution increases with time. In contrast, in the r direction the ion motion is stable. Another interesting feature is that although the motion is unstable in the z-direction the points on the Poincaré section move away from the origin approximately along three straight lines. The ion motion at these parameter values has a secular frequency of $\Omega/3$ where Ω is the frequency of the rf drive.

In Fig. 8 we do a similar analysis for our second point of interest, which is at $q_z = 0.64$ with $a_z = 0$. We have plotted the Poincare map in this case for an initial condition of $(z, r, \dot{z}, \dot{r}) = (0.0025, 0.0025, 0, 0)$. It can be seen that the ion motion grows in the z direction while in the r-direction the motion is stable. Here, again, we see that the points in the map in the z-direction lie roughly on four lines indicating that for this motion the ion secular frequency is $\Omega/4$.

Eqs. (9) and (12) are forms of the nonlinear Mathieu equation with the nonlinear terms being excited parametrically by the rf drive. Based on the Poincare maps, regions close to $q_z = 0.78$ and 0.64 where ion motion displayed a periodicity of $\Omega/3$ and $\Omega/4$, respectively, will be considered below. Recall that it was close to these points that the escape velocity displayed sharp decreases in magnitude.

As the Poincare map showed growing solutions *only* in the z-direction we will analyze, for simplicity, only the uncoupled z-equation represented as

$$\frac{\mathrm{d}^2 z}{\mathrm{d}\tau^2} + (a_z - 2q_z \cos 2\tau)\left(z + \frac{3hz^2}{r_0} + \frac{4fz^3}{r_0^2}\right) = 0 \qquad (22)$$

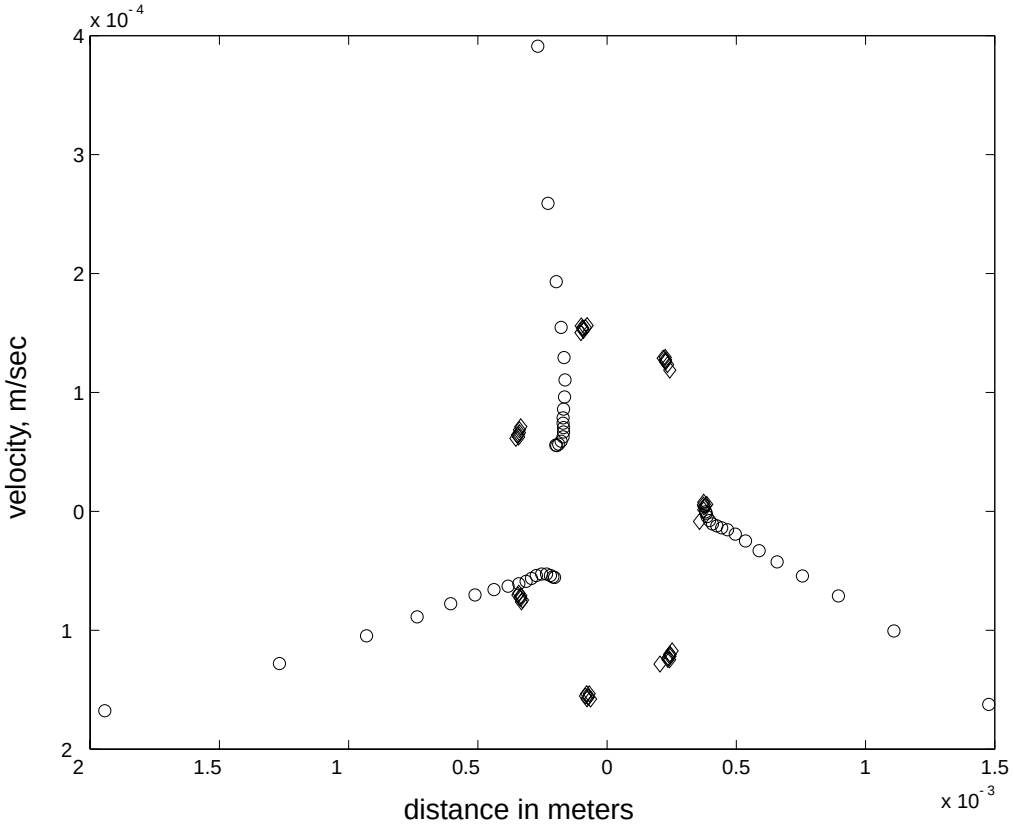

Fig. 7. Poincare map obtained at an operating point of $a_z = 0$ and $q_z = 0.78$; circles show motion in z-direction and diamonds show motion in the r-direction.

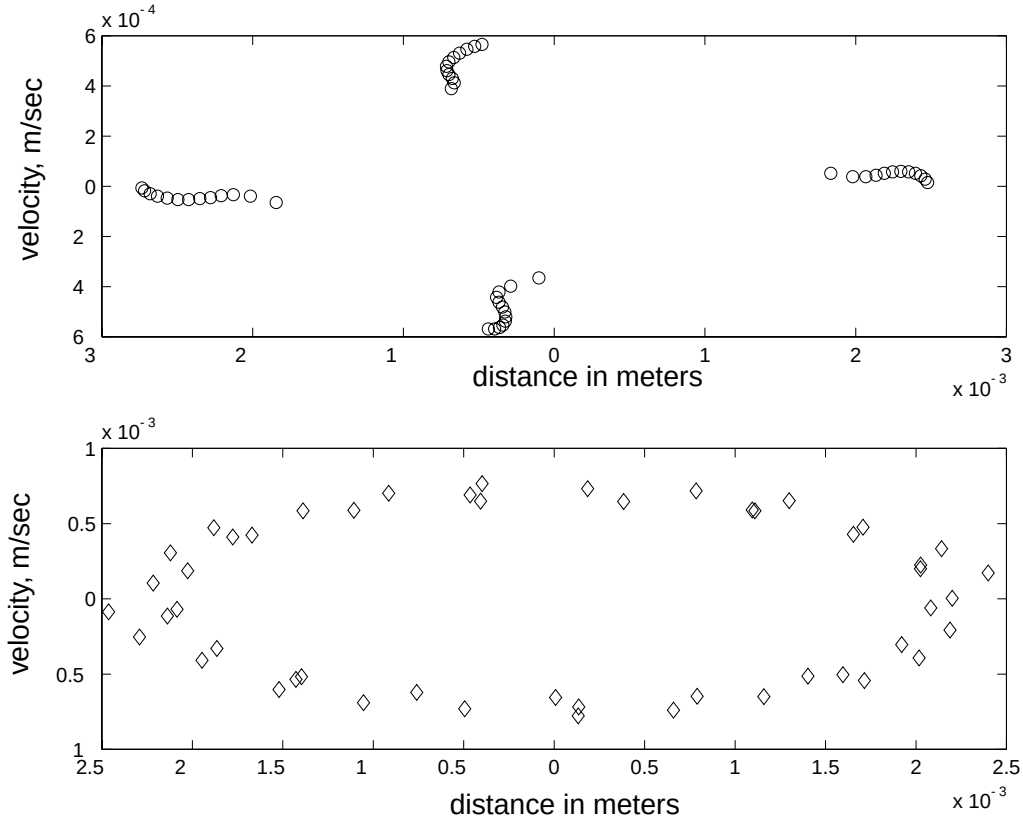

Fig. 8. Poincare map obtained at an operating point of $a_z = 0$ and $q_z = 0.64$; circles show motion in z-direction and diamonds show motion in the r-direction.

5.2.1. Ion dynamics close to the 1/3 resonance: role of hexapole nonlinearity

The equation of motion with only hexapole component as nonlinearity along the $a_z = 0$-axis can be obtained from Eq. (22) as

$$\frac{\mathrm{d}^2 z}{\mathrm{d}\tau^2} - 2q_z \cos 2\tau \left(z + \frac{3hz^2}{r_0} \right) = 0 \tag{23}$$

In order to make the amplitude comparable to unity, we rescale z as

$$\bar{z} = \frac{z}{r_0} \tag{24}$$

where r_0 is the radius of the ring electrode. Substituting Eq. (24) into Eq. (23) we get

$$\frac{\mathrm{d}^2 \bar{z}}{\mathrm{d}\tau^2} - 2q_z \cos 2\tau \left(\bar{z} + \varepsilon \bar{z}^2 \right) = 0 \tag{25}$$

where

$$\varepsilon = 3h \tag{26}$$

As we are looking for points very close to the 1/3 resonance point, we consider our trapping condition to be detuned from the exact 1/3 resonance point, the detuning being represented by a small detuning parameter Δ defined as

$$q_z = q_z^* + \varepsilon\Delta \tag{27}$$

where q_z^* corresponds to the exact value of q_z when the solution is periodic in 3π and ε denotes the small variation from this value. While ε has been defined in Eq. (26) as the perturbation term, we introduce here Δ as the detuning parameter. This helps us study ion dynamics in the neighborhood of the resonance. Variation of Δ will describe the extent of detuning of q_z from the exact resonance point. Substituting Eq. (27) into Eq. (23) and rearranging the terms to bring it to the form of Eq. (15) we get

$$\frac{\mathrm{d}^2 \bar{z}}{\mathrm{d}\tau^2} - 2q_z^* \bar{z} \cos 2\tau = \varepsilon \cos 2\tau (2\Delta\bar{z} + 2q_z^* \bar{z}^2) + O(\varepsilon^2) \tag{28}$$

where $O(\varepsilon^2)$ represents terms of order ε^2 which are neglected in our present analysis. Following [18], we get the value of $q_z^* = 0.7847$. At this value of q_z the linear Mathieu equation has a frequency equal to $\Omega/3$ and the detuning parameter Δ will be referenced to this value of q_z.

The slow flow equations obtained in this case are [18]

$$\dot{A} = \varepsilon(-1.9067AB + 1.3874\Delta B) \tag{29}$$

and

$$\dot{B} = \varepsilon(-1.3873\Delta A - 0.9509A^2 + 0.9552B^2) \tag{30}$$

Integrating Eqs. (29) and (30) gives the variation of amplitude of the cosine and sine term with time. Numerically integrating these equations, with different initial conditions,

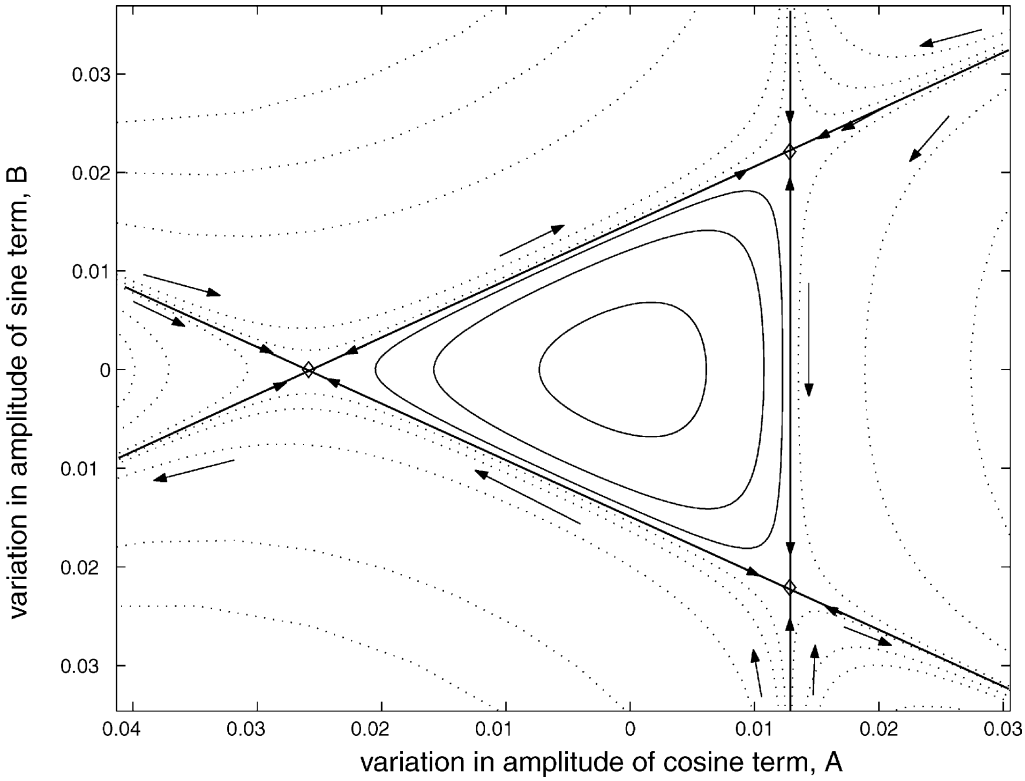

Fig. 9. Phase plot showing variation of A vs. B in the slow flow for 10% hexapole nonlinearity and a q_z value of 0.78.

for obtaining A and B we construct a phase portrait on the $A-B$ phase plane with A on the x-axis and B on the y-axis. Fig. 9 shows the phase portrait obtained by numerically integrating Eqs. (29) and (30) with 10% hexapole nonlinearity and a q_z value of 0.78. It can be seen that for small initial conditions the ion has a stable trajectory while for large initial conditions the ion becomes unstable and escapes form the trap. It can also be seen that the stable and unstable regions can be separated by a set of three straight lines that intersect to form a triangle within which the ion motion is stable. These are obtained as [29]

$$\begin{aligned} A &= 1.732B - 1.453\Delta \\ A &= -1.732B - 1.453\Delta \\ A &= -0.726\Delta \end{aligned} \tag{31}$$

Solving Eq. (31) to find the points of intersection of these straight lines we get

$$(A, B) = \begin{pmatrix} (-1.453\Delta, 0) \\ \left(0.726\Delta, \dfrac{2.167}{1.732}\Delta\right) \\ \left(0.726\Delta, \dfrac{-2.167}{1.732}\Delta\right) \end{pmatrix} \tag{32}$$

The triangle formed by joining these three points in the phase plane demarcates the stable region from the unstable region. In Fig. 9 we have also plotted the three straight lines given by Eq. (31). The points of intersection of these three lines given by Eq. (32) are marked with ◇. The direction of flow in the phase space is shown by arrows.

It is seen from Eq. (32) that the area of the triangle separating the stable region from the unstable region is dependent on the detuning parameter Δ since the points of intersection are directly proportional to it. Increase in the magnitude of Δ increases the area of stability in the phase portrait (thereby resulting in an increase in the escape velocity in our numerical computations). As the detuning parameter reduces, the stable region in the phase portrait reduces with the area going to zero at $\Delta = 0$. Therefore, at $q_z = q_z^*$ the ion is not stable for any given initial condition.

For a negative Δ ($q_z < q_z^*$) the three points of intersection of the straight lines, given by Eq. (32) changes in sign and the $A-B$ phase portrait will be similar to the one obtained for the positive Δ case but reflected on the $A = 0$ line (B-axis).

Let us next turn our attention to study the effect of change of the weight of nonlinearity on the stability of the ion. As the instability is dependent on the detuning parameter for any given hexapole nonlinearity the ion will be unstable at $q_z = q_z^*$. The rate at which the detuning parameter changes with change of q_z from q_z^* is dependent on the nonlinearity since

$$\Delta = \frac{q_z - q_z^*}{\varepsilon} \tag{33}$$

From Eq. (33) it is evident that Δ changes very fast with changing q_z for small values of nonlinearity. Hence, though the ion is unstable at $q_z = q_z^*$ for any hexapole nonlinearity,

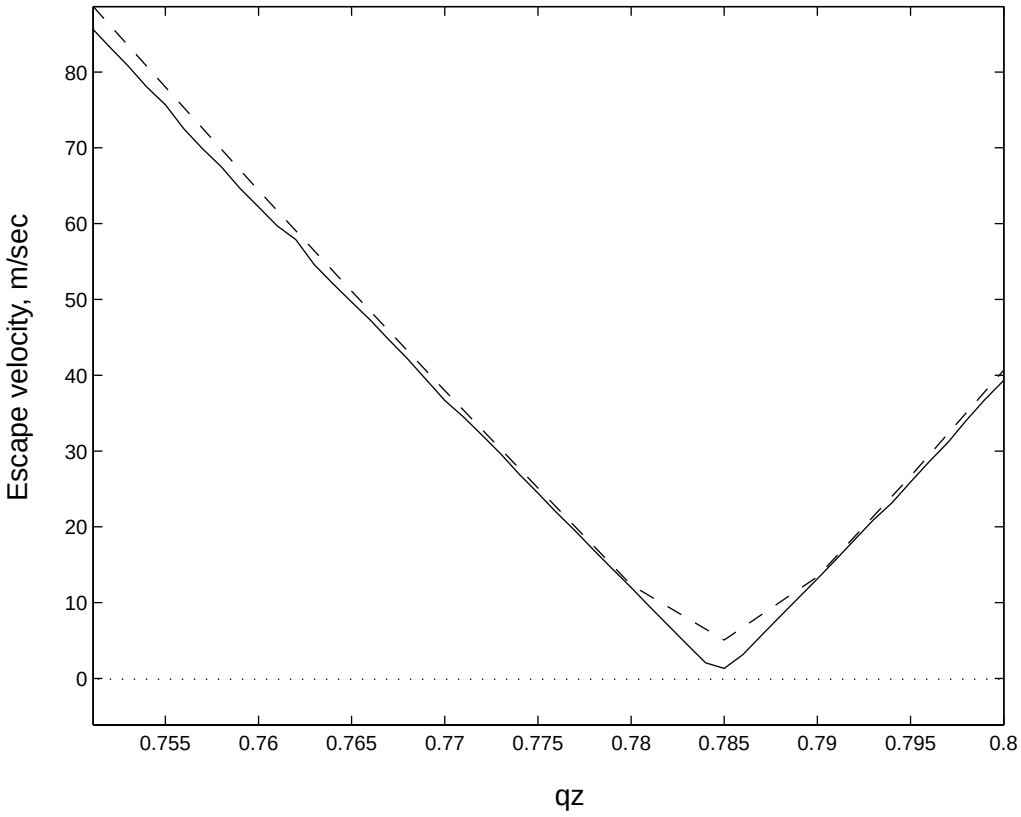

Fig. 10. Comparison of change of escape velocity for hexapole nonlinearity at the 1/3 resonance for different times. Solid line represents increase in the time by a factor of 4 as compared to dotted line.

the trapping strength increases very rapidly with any change of q_z from q_z^* for a small nonlinearity as compared to a larger nonlinearity, resulting in much sharper resonance lines for smaller nonlinearity. It may be recalled that our numerical simulations had also indicated this, showing a very sharp dip in the escape velocity for smaller nonlinearity as compared to a broad dip for higher nonlinearity with the value of the escape velocity at the minimum remaining almost the same (please refer Fig. 2). Therefore, a small hexapole nonlinearity results in a sharp nonlinear resonance ejection at the 1/3 resonance line. As the $\mathrm{d}A/\mathrm{d}B$ variation obtained from Eqs. (29) and (30) is not directly dependent on ε (it is related through the effect ε has on Δ) any change of sign of the nonlinearity will result only in a change of sign of Δ.

As an aside, let us recall that in Fig. 2, we observed that at this 1/3 resonance point, the escape velocity had a nonzero value. However, the analysis presented here suggests that the ion should indeed be unstable at that point. In order to check this latter observation, we ran the simulation for estimating escape velocity for the conditions of Fig. 2 by increasing the time by a factor of 4. Fig. 10 plots the escape velocity for this conditions (in solid line) comparing it with the earlier case (dashed line). It can be seen that when the time was increased by a factor of 4, the escape velocity reduced by the same factor. It can be seen from this comparison that the escape velocity goes to zero as the time allowed goes to infinity.

5.2.2. Ion dynamics close to the 1/3 resonance: role of octopole nonlinearity

The equation of motion with only octopole superposition along the $a_z = 0$-axis can be written (from Eq. (22)) as

$$\frac{\mathrm{d}^2 z}{\mathrm{d}\tau^2} - 2q_z \cos 2\tau \left(z + \frac{4fz^3}{r_0^3} \right) = 0 \tag{34}$$

Proceeding as before we get the slow flow as

$$\dot{A} = \varepsilon(2.1375A^2B + 1.3873\Delta B + 2.1375B^3) \tag{35}$$

and

$$\dot{B} = \varepsilon(-1.3873\Delta A - 2.1428AB^2 - 2.1350A^3) \tag{36}$$

and from Eqs. (35) and (36) we get

$$\frac{\mathrm{d}A}{\mathrm{d}B} = \frac{2.1375A^2B + 1.3873\Delta B + 2.1375B^3}{-1.3873\Delta A - 2.1428AB^2 - 2.1350A^3} \tag{37}$$

For octople nonlinearity at 1/3 resonance the phase plot obtained by Eqs. (35) and (36) (Fig. 11) show a stable structure and any instability, if present, does not appear in this first order analysis. However, an interesting feature of ion motion at this point can be seen on analyzing Eq. (37). At low amplitudes the terms with Δ dominate and the equation is similar to that of a circle. At higher amplitudes, the Δ terms lose importance as the cubic terms increase in magnitude. The equation is still that of a circle but its direction

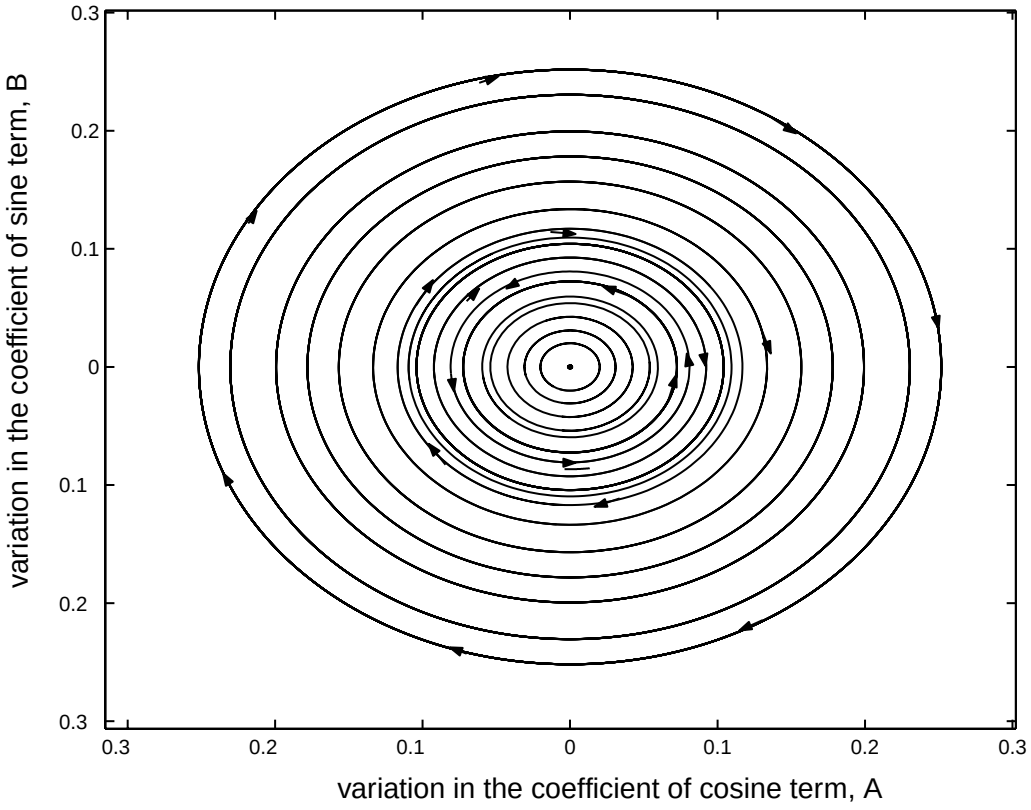

Fig. 11. Phase portrait for octopole nonlinearity 10% at $q_z = 0.78$.

changes. At the transition from clockwise to counterclockwise circles, there are some finer details which may not be reliable due to the approximations made in the analysis and which are not important from a practical point of view.

5.3. Ion dynamics close to the 1/4 resonance: role of hexapole nonlinearity

The equation of motion with only hexapole component as nonlinearity along the $a_z = 0$-axis is given by Eq. (23). Proceeding as in the earlier cases we get the exact location of the 1/4 resonance along the $a_z = 0$ line at $q_z = 0.6393$ and get the slow flow as

$$\dot{A} = \varepsilon 0.9873 \Delta B \tag{38}$$

and

$$\dot{B} = -\varepsilon 0.9873 \Delta A \tag{39}$$

This pair of equations represent a circle implying stable ion motion in the first order analysis.

5.3.1. Ion dynamics close to the 1/4 resonance: role of octopole nonlinearity

We will now turn our attention to ion dynamics close to the 1/4 resonance with octopole nonlinearity in the trap. When the type of nonlinearity is octopole we have the equation of motion as (please see Eq. (22)) along the $a_z = 0$-axis

$$\frac{\mathrm{d}^2\bar{z}}{\mathrm{d}\tau^2} - 2q_z^*\bar{z}\cos 2\tau = \varepsilon \cos 2\tau(2\Delta\bar{z} + 2q_z^*\bar{z}^3) + O(\varepsilon^2) \tag{40}$$

where q_z^* is the exact value of q_z at 1/4 resonance and $\varepsilon\Delta$ corresponds to the detuning of q_z from this value (Eq. (27)). For the octopole nonlinearity, ε is given by

$$\varepsilon = 4h \tag{41}$$

Proceeding as in the previous section we obtain $q_z^* = 0.6393$ and the slow flow equation takes the form [18]

$$\dot{A} = \varepsilon(-0.082834A^2B + 0.98731\Delta B + 1.46962B^3) \tag{42}$$

and

$$\dot{B} = \varepsilon(-0.98731\Delta A + 0.082834AB^2 - 1.46962A^3) \tag{43}$$

The effect of detuning parameter Δ and the strength of nonlinearity ε on the equation of motion can be studied by numerically integrating Eqs. (42) and (43) for different initial conditions. When Δ is zero or positive the phase portrait shows closed curves around the center of the trap. When Δ becomes negative the number of fixed points in the phase plane increases to nine of which four are saddles; the remaining five are centers, of which one is at the origin. There are also larger orbits that inscribe all nine fixed points. The $A - B$ phase space for one such negative Δ is shown in Fig. 12, for $q_z = 0.63$ and a octopole nonlinearity of 10%.

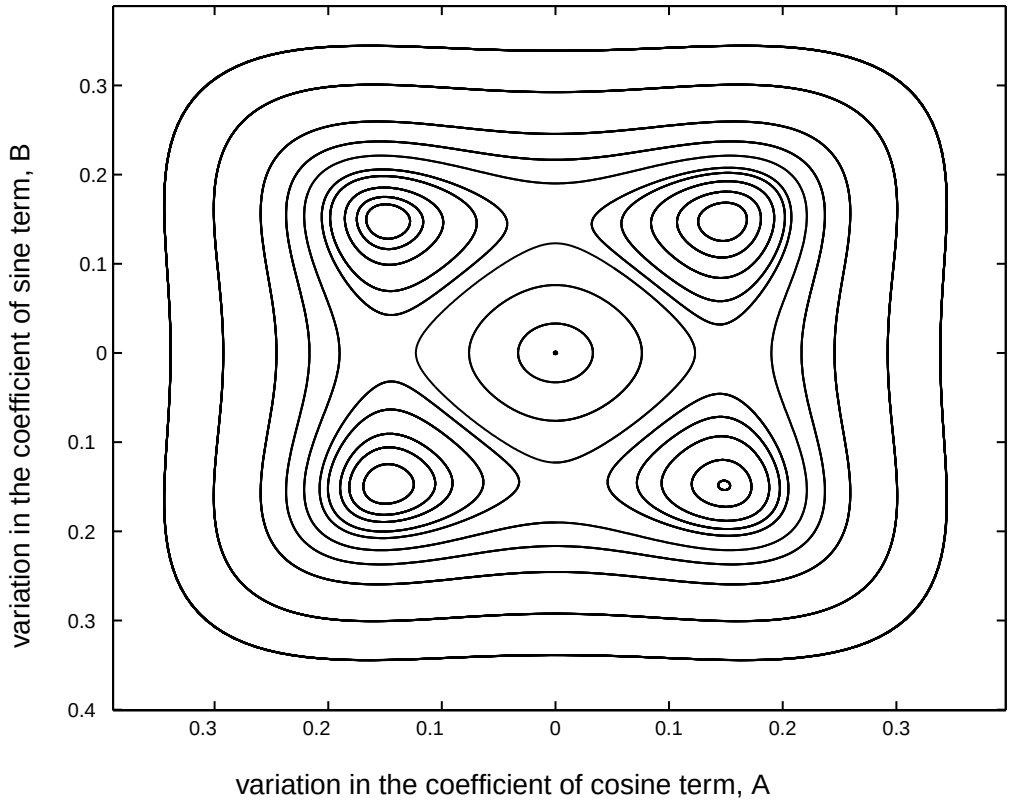

Fig. 12. Phase plot showing variation of A vs. B in the slow flow for 10% octopole nonlinearity and a q_z value of 0.63.

We will now, based on the observations presented above, explain the reduction in trapping strength near the 1/4 resonance in light of the qualitative dynamics as seen in Fig. 12. A portion of that figure is sketched in Fig. 13, which shows the center at O, two saddles at M and N, two heteroclinic orbits (also separatrices) MCN and MDN; these will be discussed below.

From Eqs. (42) and (43), for negative Δ, we can see that Fig. 12 scales in size proportionally to $\sqrt{|\Delta|}$. With this insight, let us start at a small value of $|\Delta|$, and slowly increase it. Initially, the trap dimensions are large compared to the scaled Fig. 12. At this stage, a large initial condition is needed for the ion to reach the trap geometry, and the escape velocity is not small. As Δ is decreased (or $|\Delta|$ is increased), the scaled Fig. 12 grows in size. Eventually, for some Δ, the trap boundary is reached by an ion whose A and B value correspond to the point R in Fig. 13. At this point, the escape velocity corresponds to the point[2] S. On decreasing Δ slightly further, the scaled Fig. 12 gets slightly bigger, and now the ion at point Q reaches the trap boundary. However, to reach point Q, the ion need not start any further from the origin than point P, where we note that the distance OP is significantly less than OS. Thus, at some specific negative value of Δ, the trapping strength should drop sharply, as has been seen earlier using numerics. Now, on decreasing Δ slightly further, the scaled Fig. 12 grows bigger. Escape now corresponds to the trajectory reaching a distance OQ. However, the trajectory starting from P reaches that far and beyond, and so the escape velocity continues to correspond to distance OP. Note that, due to the increase in size of Fig. 12, distance OP grows with $|\Delta|$, and so in this range of Δ we find the escape velocity increasing with $|\Delta|$, as also seen in the numerics. Eventually, the trap dimension

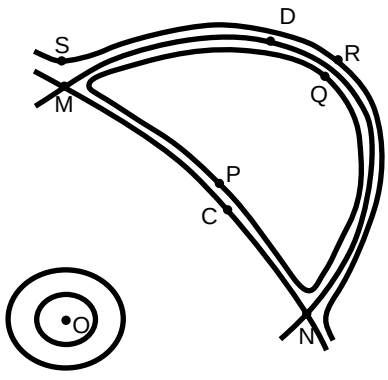

Fig. 13. Schematic of a portion of Fig. 12.

[2] Actually, the point S represents a periodic motion of the ion. This periodic motion crosses the trap center two or more times within each period. At each such crossing, the ion has some velocity. The least of these velocities is the escape velocity (the other velocities correspond to escape starting from different phases of the forcing cycle). However, it is easy to show that this escape velocity is in fact proportional to the distance OS.

crosses inside the separatrix MCN, and then there are simple periodic orbits encircling the origin O. In this range, the escape velocity becomes roughly constant (stops changing significantly with Δ).

Finally, we consider what happens if we reduce the magnitude of the nonlinear term. Now, when ε becomes smaller, for the same value of physical detuning $\varepsilon\Delta$, the mathematical value of Δ will become larger. Thus, we expect that the width of the region of reduced trapping strength will become smaller with smaller nonlinearity. This too matches our numerical observations.

6. Concluding remarks

Through this study we have attempted to understand the role of field inhomogeneties in altering stability of ions within the nominally stable region of the Mathieu stability plot. The study used the concept of escape velocity to profile trapping strengths and to present comparative results of the difference in trapping strengths associated with different nonlinear resonances. An analytical study at two "weak" regions has also been carried out to understand dynamics of ions during destabilization.

The numerical studies to estimate escape velocities adequately profiled the experimentally observed variations of trapping strengths reported in literature and further enabled the understanding of how magnitude and sign of nonlinearity influences trapping strength. What was also evident was that reducing nonlinearity does not necessarily increase escape velocity (and hence the trapping strength) for all nonlinear resonances as was exemplified by the influence of hexapole superposition at $\beta = 2/3$ resonance. It was also seen that studies carried out at nonzero values of a_u showed the influence of field inhomogeneities on trapping strength throughout the stability plot. In principle, inclusion of terms in the governing equation beyond those corresponding to octopole nonlinearity, could give an insight into nonlinear resonances which may not have appeared in our computations but which may have been observed in experimental studies.

The novel technique of harmonic balance based averaging used in our analytical studies helped us in distinguishing the destabilization dynamics associated with two nonlinear resonances on the Mathieu stability plot. At one of those points the analysis showed that the ion is inherently *unstable* while at the other point the phase portrait indicated that although the ion is intrinsically *stable*, the multiplicity of centers provided an easy escape path for the trapped ion. It was also possible to associate the influence of specific field inhomogeneties in bringing about ion destabilization. For two other conditions, corresponding to 1/3 resonance and octopole nonlinearity and 1/4 resonance and hexapole nonlinearity, our current analysis did not show any inherent instability though the numerical analysis suggested a decreased trapping strength for at least one of these cases. We suspect that this could be a limitation of the first order analysis used here.

An anonymous reviewer suggested that our observation of the inherent stability (or boundedness of motions) of the ion in the presence of octopole nonlinearity is related to Franzen et al.'s [7] observation that the octopole resonance can quench itself due to shifting of secular frequencies with growth in oscillation amplitude. The relation between Franzen et al.'s [7] observation and ours can be seen through our Fig. 6 which shows shifting of the minima in escape velocity to the left or right depending on whether the octopole nonlinearity is positive or negative, respectively. Note that the amount of shift depends on the strength of the nonlinearity as seen in our analysis; however, given a certain nonlinear field, the effective nonlinearity grows directly with the amplitude, which leads to the observation of [7].

Acknowledgements

Anindya Chatterjee was partially supported by ISRO and DRDO through the Nonlinear Studies Group at IISc. We are grateful to two anonymous reviewers for their suggestions.

References

[1] R.E. March, R.J. Hughes, Quadrupole Storage Mass Spectrometry, Wiley-Interscience, New York, 1989.
[2] P.H. Dawson, Quadrupole Mass Spectrometry and its Application, Elsevier, Amsterdam, 1976.
[3] H.G. Dehmelt, Adv. At. Mol. Phys. 3 (1967) 53.
[4] F.G. Major, H.G. Dehmelt, Phys. Rev. 170 (1967) 91.
[5] R.E. March, Int. J. Mass Spectrom. Ion Process. 118/119 (1992) 72.
[6] J. Louris, J. Schwartz, G. Stanfford, J. Syka, D. Taylor, in: Proceedings of the 40th ASMS Conference on Mass Spectrometry and Allied Topics, Washington, DC, 1992, p. 1003.
[7] J. Franzen, R.H. Gabling, M. Schubert, Y. Wang, Non-linear ion traps, in: R.E. March, J.F.J. Todd (Eds.), Practical Aspects of Ion Trap Mass Spectrometry, CRC Press, New York, 1995, Chapter 3, p. 49.
[8] K.A. Cox, C.D. Cleven, R.G. Cooks, Int. J. Mass Spectrom. Ion Process. 144 (1995) 47.
[9] X. Luo, X. Zhu, K. Gao, J. Li, M.Yan, L. Shi, J. Xu, App. Phys. B 62 (1996) 421.
[10] J.F.J. Todd, R.M. Waldren, R.E. Mather, Int. J. Mass Spectrom. Ion Phys. 34 (1980) 325.
[11] J.F.J. Todd, R.M. Waldren, R.E. Mather, Int. J. Mass Spectrom. Ion Phys. 35 (1980) 107.
[12] F. Guidugli, P. Traldi, Rapid Commun. Mass Spectrom. 5 (1991) 343.
[13] K.L. Morand, S.A. Lammert, R.G. Cooks, Rapid Commun. Mass Spectrom. 5 (1991) 491.
[14] F. Guidugli, P. Traldi, A.M. Franklin, M.L. Langford, J. Murrel, J.F.J. Todd, Rapid Commun. Mass Spectrom. 6 (1992) 229.
[15] R. Alheit, S. Kleineidam, F. Vedel, M. Vedel, G. Werth, Int. J. Mass Spectrom. Ion Process. 154 (1996) 155.
[16] Y. Wang, J. Franzen, K.P. Wanczek, Int. J. Mass Spectrom. Ion Process. 124 (1993) 125.
[17] A. Chatterjee, Nonlinear Dyn. 32 (2003) 323.
[18] G.T. Abraham, A. Chatterjee, Nonlinear Dyn. 31 (2003) 347.
[19] E.C. Beaty, Phys. Rev. A 33 (1986) 3645.
[20] M. Sudakov, Int. J. Mass Spectrom. 206 (2001) 27.
[21] S. Sevugarajan, A.G. Menon, Int. J. Mass Spectrom. 218 (2002) 181.

[22] L.N. Virgin, L.A. Cartee, Int. J. Non-Linear Mech. 26 (1991) 449.
[23] MATLAB Reference Guide, The Math Works Inc., Natick, 1992.
[24] E. Alheit, X.Z. Chu, M. Hoefer, M. Holzki, G. Werth, Phys. Rev. A 56 (1997) 4023.
[25] M. Vedel, J. Rocher, M. Knoop, F. Vedel, Appl. Phys. B 66 (1998) 191.
[26] N.W. McLachlan, Theory and Applications of Mathieu Functions, Oxford University Press, UK, 1947.
[27] M. Abromowitz, I.A. Stegun, Handbook of Mathematical Functions, Dover, New York, 1970.
[28] K.M. Heal, M.L. Hansen, K.M. Rickard, Maple 6.0, Learning Guide, Waterloo Maple Inc., Canada, 2000.
[29] G.T. Abraham, Escape Velocities and Ejection via Nonlinear Resonances in Paul Traps, Unpublished M.Sc. (Eng.) Thesis, Department of Instrumentation, Indian Institute of Science, Bangalore, India, 2002.